International Journal of Science and Research (IJSR)
ISSN (Online): 2319-7064
Index Copernicus Value (2013): 6.14 | Impact Factor (2013): 4.438

Effect of Reactive Magnesia on the Properties of Alkali Activated Slag Cement Pastes

H.A. Abdel-Gawwad[1], S. Abd El-Aleem[2]

[1]Housing and Building National Research Center, Giza, Egypt,

[2]Chemistry Department, Faculty of Science, Fayoum University, Fayoum, Egypt

Abstract: ***The effect of different proportions of different reactive magnesium oxides (MgOs) on the compressive strength and drying shrinkage of alkali activated slag pastes (AASPs) has been investigated. The slag was activated by 6 wt., % of sodium hydroxide (SH) and liquid sodium silicate (LSS) at a ratio of 3:3 wt., %. The MgOs with different reactivities were produced from calcination of hydromagnesite at different temperatures (550, 1000, and 1250°C). The results show that, the crystallinity of MgO increases with the calcination temperature, therefore its reactivity decreases with temperature. The highly reactive MgO_{550} accelerates the hydration and consequently increases the early compressive strength of AASPs, while the low reactive MgO_{1250} had little effect. The acceleration of AAS-MgO hydration at early ages is mainly due to the exothermic hydration reaction of MgO. The replacement of GBFS by 5 wt., % of low reactive MgO_{1250} significantly improves the compressive strength at later curing ages. The replacement of slag by 5, 10 and 15 % of MgO_{550} reduces the drying shrinkage of AASPs by ~40, 57 and 77%, respectively after 90 days. Also, the drying shrinkage of AAS is reduced by replacement of slag with different reactive MgOs. The MgO reacts with slag to form hydrotalcite like- phases (Ht) as detected by XRD, FTIR and TG/DTG techniques.***

Keywords: Reactive magnesium oxide, calcination temperature, drying shrinkage, hydrotalcite like-phases, magnesium silicate hydrate

1. Introduction

Recently, alkali-activated slag (AAS) binders have taken a great interest due to the lower energy requirements and lower emission of greenhouse gases as compared to Portland cement (PC) manufacturing. Production of cement accounts for about 5% of the global total CO_2 emissions **[1], [2]**. Reduction of energy usage can be taken place even by design methods **[3]** or using supplementary cementitious materials (SCMs) (e.g., granulated blast furnace slag (GBFS), fly ash (FA), and silica fume) in cement concrete, either as a mineral admixture or a component of blended cement **[4]**.

Blast furnace slag (BFS) is a by-product generated from the manufacture of pig iron. It forms when the slagging agents (e.g., iron ore, coke ash and limestone) are added to the iron ore to remove the contaminated impurities. In the process of reducing iron ore to iron metal, a molten slag forms as nonmetallic liquid (consisting primarily of silicates and aluminosilicates of calcium and other elements) that floats on the top of the molten iron. The molten slag is then separated from the liquid metal and cooled by different methods. When the slag is allowed to cool slowly in the air, it solidifies into crystalline material known as air-cooled slag (ACS). But, when it is rapidly and sufficiently cooled by water, it solidifies into granulated form, which known as water cooled slag (WCS) or granulated blast furnace slag (GBFS). The chemical composition of slag can vary over a wide range depending on the nature of the ore, the composition of the limestone flux, coke consumption and the type of iron being made. The main constituents of slag include: CaO, SiO_2 and Al_2O_3. In addition, it contains small amount of MgO, FeO and sulphides as CaS, MnO and Fe, which are the most common components in commercial silicate glasses **[5]**

In previous works **[6]-[8]**, it was concluded that, indicate that, AAS cements and concretes present high mechanical strength and good performance in chemical attack, frost/thaw cycles and high temperatures. The main application of these binders is in pre-casting and repairing.

Cincotto et al **[9]** reported that, AAS mortars and concretes are subjected to substantial autogenous and drying shrinkage; this is one of the main drawbacks of definitive use of AAS as an alternative to traditional PC binder. From the main factors that affecting the drying shrinkage of AAS, are the type and content of alkali activator, the properties of aggregate and slag **[10]**, as well as curing environment **[11]**. In general, water–glass activated slag has more shrinkage than sodium hydroxide activated slag and the drying shrinkage of AAS increases with the activator dosage as well as slag fineness **[12]**. In addition, the shrinkage of AAS is very sensitive to the curing conditions. It is reported that, the drying shrinkage of AAS concrete is similar to that of PC-concrete at 70% relative humidity (RH), and it is significantly higher at 33 and 50% RH than that of PC-concrete **[13], [14]**.

Bakharev et al. **[15]** studied the effect of different admixtures on water glass-activated slag concrete. They found that, lower drying shrinkage (at 50% RH) was observed for the AAS concrete compared to PC concrete prepared with 6 mass, % of gypsum. It was concluded that, gypsum reduces both autogenous and drying shrinkage, due to the formation of high expansive phases such as ettringite (AFt). The specimens containing superplasticizer showed the highest drying shrinkage, followed by those without admixtures, and then those with water-reducing admixtures, whilst the specimens containing air-entraining agent exhibited the lowest shrinkage.

The use of magnesia, MgO, as a shrinkage reducing additive, dates back to the mid-1970s in the construction of

the Baishan concrete arch gravity dam **[16]**, where it proved to be a more efficient and economical admixture for controlling the shrinkage of PC than conventional admixtures **[17]**. The volume compensation during the drying process was due to the reaction between MgO and water to form brucite $Mg(OH)_2$, which results in 118% volume increase **[18]**. The effect of MgO in the AAS-systems has recently been investigated, either in terms of its varying natural content in different slag compositions **[19]**, or as an additive **[20]**. The MgO naturally present in slags is categorized as dead burned MgO (Periclase); whereas reactive grade MgO (calcined at temperature lower than 1000°C) or hard burned MgO (calcined at 1000–1400°C) are often chosen as additives **[21]**.

The effect of natural MgO content in different slags on the performance of AAS was investigated **[19]**. The results showed that, the main hydration product of AAS-MgO system is still calcium silicate hydrate (CSH) gel. The MgO molecules react with slag to form hydrotalcite, (Mg_6 Al_2 $(OH)_{16}$ $CO_3.4H_2O$)-like phases, which increases with the MgO percentage. The hydrotalcite phases are more voluminous than CSH, resulting in higher strength, therefore the higher the MgO content, the higher the strength.

Fei Jin et al. studied the effect of addition of commercial reactive MgO on drying shrinkage and strength of AAS. They are found that, the highly reactive MgO accelerated the early AAS hydration, while MgO with medium reactivity had little effect **[22]**.

The drying shrinkage was significantly reduced by highly reactive MgO but it also, generated severe cracking under the dry condition. Medium-reactive MgO only showed observable shrinkage-reducing effect after one month, but the cement soundness was improved. The hydration products were analyzed by XRD, TGA and SEM techniques. It was concluded that, Mg was mainly incorporated in the hydrotalcite-like phases. The curing conditions, the time of hydrotalcite formation and their quantity are crucial to the developed strength and shrinkage reduction of AAS-MgO binder, which are highly dependent on the reactivity and content of MgO.

In this work the effect of reactive magnesia (produced from hydromagnesite calcination at different elevated temperatures) on the physico-mechanical properties of AAS was studied.

2. Materials and Experimental Techniques

2.1. Materials

Granulated blast-furnace slag (GBFS) was supplied from Iron and Steel Company, Helwan, Egypt. Hydromagnesite (HM) was purchased from Arabic Chemical Company, Egypt. Sodium hydroxide (SH) powder of 99 % purity was obtained from Fisher Scientific Company, UK. Liquid sodium silicate (LSS) with 17 % Na_2O, 32 % SiO_2 and density of 1.46 was obtained from El Gomhourya Chemical Company, Egypt. The chemical compositions of GBFS and hydromagnesite as determined by X-ray fluorescence (XRF) were listed in Table (1). The mix composition of GBFS-MgO blends, alkali activator content and calcination temperature were given in Table (2). The mineralogical compositions of GBFS and HM are plotted in Fig. (1). It is clear that, GBFS is mainly amorphous and HM is well crystalline composed of 100 % HM without any impurities.

Fig. (2) shows the particle size distribution of GBFS, HM and MgO, produced from HM calcination at different temperatures, (550, 1000 and 1250°C). It is can be found that, GBFS has 90 % of the paricle size < 50 µm and 10 % < 7 µm. On the other side, the particle size of HM is mainly lower than 15 µm. The grain size of MgO produced from HM calcination at 550 °C (< 7 µm) is lower than those produced at 1000 °C (< 8 µm) and 1250 °C (< 11µm).

2.2. Experimental Techniques

2.2.1. Calcination of hydromagnesite (HM)

The differential thermal analysis (DTA) thermogram of HM is graphically shown in Fig. (3). The endotherms located at 68-280°C are due to dehydration and dehydroxylation of HM. The carbonate is decomposed at 425-486 °C **[23]**. Decomposition of hydromagnesite takes place as the follows:

$$Mg_5[(CO_3)_4(OH)_2].4\,H_2O \rightarrow Mg_5[(CO_3)_4(OH)_2] + 4\,H_2O \quad (1)$$

$$Mg_5[(CO_3)_4(OH)_2] \rightarrow 4\,MgCO_3 + MgO + H_2O \quad (2)$$

$$4\,MgCO_3 \rightarrow 4\,MgO + 4\,CO_2 \quad (3)$$

In order to study the effect of different calcination temperatures on the reactivity and crystallinity of magnesium oxide, the hydromagnesite was calcined at 550, 1000 and 1250°C.The MgO calcined at temperatures 550, 1000 and 1250 namely MgO_{550}, MgO_{1000} and MgO_{1250}, respectively. The XRD diffractograms of MgO produced from HM calcination at different temperatures from 550 up to 1250 are shown in Fig. (4). It is obvious that, the crystallinity degree of MgO increases with calcination temperature.

The duration time required for the neutralization of an acidic solution (0.25M acetic acid) with 5.0 g of a certain MgO (MgO_{550}, MgO_{1000} or MgO_{1250}) in presence of Phenolphthalein as acid-base indicator **[21]**. The time consumed from MgO addition to the change of the solution color is inversely proportional with MgO reactivity; the shorter time means more reactive MgO. The test was performed in triplicates for each sample and the average value was taken.

2.2.2. Preparation of alkali activated slag–MgO pastes

Three AAS-MgO pastes were prepared in which MgO_{550} content varied from 5 to 15 % by mass of slag. Also, two AAS-MgO mixes containing 5 mass, % of MgO_{1000} and 5 mass, % MgO_{1250} were prepared as seen in Table (2). All other components were kept constant including water to solid (GBFS, MgO and activators) ratio of 0.30 to ensure standard workability. The MgO was first mixed with GBFS for 2 min in a bench-top mixer to achieve complete homogeneity, then the 3:3 wt., % of NaOH:LSS, dissolved in mixing water, was added. The NaOH and LSS percentage was chosen as described elsewhere **[24], [25]**. After mixing

for another 2 min, the mix was cast into the cubic (25 × 25 × 25 mm) or prism (25×25×285 mm) moulds in two layers and manually-vibrated to eliminate air voids. The samples were then covered to avoid moisture loss. After 24 h, the specimens were carefully demoulded and transferred into the relative humidity chamber of 99 ± 1 % at 23 ± 2°C.

2.2.3. Compressive strength and drying shrinkage

Three specimens of each AAS-MgO blend were tested for compressive strength and drying shrinkage measurements. The compressive strength was measured after 1, 7, 14, 28, and 56 days of curing according to ASTM C109M **[26]**. Shrinkage was determined according to ASTM C490 **[27].** The length change of activated slag mortar with or without MgO at any curing age was calculated as follows: $L = (L_x - L_i) / G$ where: L_x = comparator reading of specimen at x age minus comparator reading of reference bar at x age. L_i = initial comparator reading of specimen minus comparator reading of reference bar at zero time. G = nominal gauge length of 285 mm.

Differential thermal analysis (DTA) and thermogravimetric analysis (TGA) were carried out by heating the sample in nitrogen atmosphere up to 1000°C with a heating rate 20°C/min using a DT-50 Thermal Analyzer (Schimadzu Co-Kyoto, Japan). XRD analysis was carried out on a Philips PW3050/60 X-ray diffractometer using a scanning range from 5 to 50 2θ degrees with a scanning speed of 1second/step and resolution of 0.05°/step. Infrared spectral analysis (FTIR) was carried out for some selected hydrated samples to provide additional information on the phase transition. The FTIR was recorded from KBr discussing Genesis-IIFT-IR spectrometer in the range of 400-4000 cm^{-1}.

3. Results and Discussion

3.1. Reactivity determination of MgO

The neutralization times of different reactive MgOs (MgO_{550}, MgO_{1000} or MgO_{1250}) tested with 0.25 M acetic acid are plotted in Fig. (5). It is clear that, the times required to neutralize acetic acid by MgO_{550}, MgO_{1000} and MgO_{1250} are 37, 70 and 163 sec, respectively. This indicated that, the MgO_{550} was more reactive than MgO_{1000} and MgO_{1250}.This proves that, the reactivity of the MgO is strongly affected by calcination temperature **[28]**.

3.2. Compressive strength measurement

Fig. (6 a) shows the effect of MgO_{550} content (5, 10 and 15 mass, %) on the compressive strength of hardened AAS pastes. The results indicated that, there is a significant development in the compressive strength at early curing ages for the pastes containing 5 mass, % MgO_{550}. The reduction in compressive strength was observed with 10 and 15 mass, % MgO_{550} (M10-550 and M15-550), but still greater than that of reference sample (M0) at 1 day. The 5 mass, % MgO_{550} increases the early age strength up to 7 days, while the 10 and 15 mass, % MgO_{550} increase the early age strength for only 1day. The M5-550 showed nearly the same strength compared to M0 after 28 and 90 days. But the compressive strengths for M10-550, M15-550 were reduced by about 22 and 30 % at 28 days, respectively and 25, 32% at 90 days compared to reference sample (M0).

Fig. (6 b) repesents the effect of MgO reactivity (MgO550, MgO1000 or MgO1250) on the strength of hardened AAS pastes. The results show that, the replacement of AAS by 5 mass, % MgO_{1250} has a little effect on strength at early curing ages (1 and 7 days). The compressive strength of AAS-MgO_{550} blend at 1 and 7 days are higher than those of M0, M5-1000, and M5-1250 blends. A significant increase in strength was observed after 7 days when AAS is replaced by 5 mass, % MgO_{550}. It can be concluded that, the highly reactive MgO accelerates the hydration of GBFS at early ages as a result of the exothermic hydration reaction of MgO, leading to the formation of excessive hydration products **[22]**. Liska **[29]** found that, the heat of hydration of high reactive MgO was nearly 25 times higher than that of less reactive MgO. It was also reported that, the temperature released during the hydration of high reactive MgO, increases to ~100°C in 30 min. The replacement of GBFS by 10 and 15 mass, % of high reactive MgO decreases the compressive strength at later ages. This may be due to that, MgO reacts with broken Si-O or Al-O in AAS matrix to form magnesium silicate hydrate (Mg-S-H) or hydrotalcite like phase (Ht), leading to the decrease of the active species, AlO_4^- and SiO_4^-, which act as monomers for C-S-H and C-A-S-H polymerization. In addition, the replacement of GBFS with high MgO_{550} percentage reduces the aluminosilicate content of AAS.

3.3. Drying shrinkage

The variation of drying shrinkage of AAS-MgO pastes with the reactivity and content of MgO is graphically shown in Fig. (7). It is obvious that, the drying shrinkage of the investigated pastes containing MgO_{550}, decreases by ~ 40, 57, and 77 %, for M5-550, M10-550, and M15-550, respectively compared to M0 after 90 days. There is no a great difference in the drying shrinkage values of M5-1000 and M5-550, especially at later curing ages. In contrast, the drying shrinkage of M5-1250 is nearly close to that of M0 during the first week, then showing a decrease in shrinkage value by ~ 15 % at 90 days than M0. It can be concluded that, the drying shrinkage reduction of AAS in presence of MgO is mainly due to the expansion caused by Ht, which formed during the hydration and carbonation of MgO **[20]**. The Ht causes healing of cracks resulted from AAS shrinkage; the healing property of Ht is attributed to its lower density ($2g/cm^3$) compared to tobermorite like CSH ($2.23g/cm^3$), leading to the formation of a uniform and compact microstructure with more effective pore filling and low porosity **[19]**. The formation rate of Ht increases with MgO reactivity since the fast hydration rate of MgO results in the Mg^{2+} being available to react with broken Al-O species in AAS matrix **[30]**.

3.4. XRD analysis

The XRD patterns of AAS with and without reactive MgO after 1 and 28 days of hydration are plotted in Fig. 8 (a, b). It can be observed that, two main hydration products (Ht and CSH) were detected. The broad beak in the range of 25–35°

2θ is related to $CaO–Al_2O_3–MgO–SiO_2$ glass structure of slag. The intensity of Ht peak in case of M5-550 is higher than that of M5-1250. This indicates that, the MgO_{550} reactivity is higher than MgO_{1250}. In addition, the high content of unreacted MgO was detected in pastes containing $MgO_{1250,}$ as a result of its lower reactivity. The intensity of CSH peak increases with curing time **[31]**. As the MgO_{550} mass, % increases, the Ht peak intensity enhances. Also, the MgO peak intensity decreases with time, due to the formation of more amount of Ht. The figure also shows that, there is no brucite present in all investigated mixes. This confirms that, MgO reacts with Si–O and Al–O (produced from alkali activation of slag), forming Mg-S-H or Ht **[32]**, but Mg–S–H is hard to be detected by XRD **[33]**.

3.5. Thermo-gravimetric and derivative thermo-gravimetric analysis (TG/DTG)

The TG/DTG thermograms of pastes cured for 1 and 28 days are represented in Figs. 9 (a, b) and Fig. 10 (a, b), respectively. It can be seen that, the weight loss at 250°C, is attributed to the dehydration of CSH and Mg–S–H **[30]**. The endotherm at the temperature range of 250–500°C corresponds to the Ht decomposition. The small peak at around 520–570°C is due to the dehydration of Mg–S–H **[34]**. The peak at 600–900 °C refers to the dissociation of Ht **[35]** and carbonate containing phases **[36]**. The intensities of Ht, CSH, and Mg-S-H peaks increase with MgO content as well as curing time. This is due to the increase of hydration rate of slag with MgO content. At 1 and 28 days of hydration, the weight loss of M15-550 (10.34 and 12.03 %) is greater than those of M5-550 (8.31 and 9.46 %) and M0 (7.71 and 8.89 %) for 1 and 28 days, respectively. On the other side, the weight loss of M5-1250 (7.03 %) is lower than that of M5-550 (8.31 %) at 1 day; this indicates the low reactivity of MgO_{1250}, which leads to the formation of low amount of Ht and Mg-S-H. The weight loss of M5-1250 (10.36%) is greater than those of M0 (8.89%) and M5-550 (9.46 %) at 28 days. It can be concluded that, MgO_{550} remarkably accelerates the slag hydration at 1 day, while the MgO_{1250} has little effect. At 28 days, both MgO_{550} and MgO_{1250} increase the hydration rate of slag.

3.6. Fourier transformer infrared (FTIR) spectroscopy

Fig. 11 (a, b) represents the FTIR spectra of AAS with and without reactive MgO at 1 and 28 days. The results show absorption band at 464-492 cm^{-1}, which is due to bending vibration of O–Si–O bonds. The well-resolved band at 658-716 cm^{-1} is associated to the symmetric stretching vibrations of Si–O–Al bridges. The absorption band located at the range of 952-974cm^{-1} seems to be due to asymmetric stretching vibrations of Si–O–T (where, T is Al or Si). The absorption band located at 1640-1649 cm^{-1} refers to the bending H-O-H vibration. But, the absorption band around 3450cm^{-1} is mainly related to stretching vibration of O-H groups. The absorption bands located at 1382-1465cm^{-1} refer to carbonate group in $CaCO_3$, $MgCO_3$ or Ht. Also, it can be observed that, the intensities of characteristic absorption bands for bending H-O-H vibration and stretching vibration of O-H group increase with curing time for all mixes. This is attributed to the continuous activation of slag hydration and formation of successive hydrated products with time.

The intensities of absorption bands referred to symmetric stretching vibrations of Si–O–Al and asymmetric stretching vibrations of Si–O–T bonds decrease with MgO_{550} content for 1 and 28 days of curing. These prove the reaction between the activated species (Al-O and Si-O) and MgO, which leads to the formation of Mg-S-H and Ht. This can be observed from the intensities of the bands related to bending H-O-H vibration and stretching of O-H groups which increases with of MgO_{550} content. The increase of the replacement level of GBFS with MgO_{550} leads to decrease the intensity of aluminosilicate bands, due to the reaction of MgO with aluminosilicate minerals. It is well observed that, the intensity of bands related to Si–O–Al symmetric stretching vibration and Si–O–T asymmetric stretching vibration of M5-1250 are higher than those of M5-550, especially after 28 days. Also, the high full width at half maximum (FWHM) of Si–O–T asymmetric stretching vibration band of M5-1250 is lower than those of M5-550 and M0. This is attributed to the low reactive MgO_{1250}, which acts as nucleation centers and accelerates the crystallization rate, reflecting on the increase of M5-1250 strength after 28 days of hydration **[37].**

4. Conclusion

The main findings of this study can be summarized as follows:

1) The crystallinity of MgO increases with the calcination temperature, therefore its reactivity decreases with temperature.
2) The highly reactive MgO_{550} accelerates the hydration and consequently increases the early compressive strength of AAS pastes, while the low reactive MgO_{1250} had little effect.
3) The acceleration of hydration of AAS- MgO at early ages is mainly due to the exothermic hydration reaction of MgO.
4) The replacement of GBFS by 5 mass, % of low reactive MgO_{1250} significantly improves the compressive strength at later ages of curing.
5) The replacement of slag by 5, 10 and 15 % MgO_{550} reduced the drying shrinkage of AAS by ~40, 57 and 77% after 90 days. Also, the drying shrinkage results of M5-1000 show nearly the same value of M5-550, especially at later ages. The drying shrinkage of low reactive MgO_{1250} (M5-1250) is comparable that of M0, then the final shrinkage (at 90 day) of M5-1250 is decreased by 15% than that of M0.
6) The MgO reacts with GBFS to form Ht like phases which is responsible for the reduction of drying shrinkage of AAS as indicated by XRD, TG/DTG, and FTIR analyses.

References

[1] K. Gu, F. Jin, A. Al-Tabbaa, B. Shi, and J. Liu, "Mechanical and hydration properties of ground granulated blast furnace slag pastes activated with MgO–CaO mixtures", Constr. Build. Mater., 6 (30); (2014), pp. 101-108.

[2] M. Heikal, M.Y. Nassar, G. El-Sayed, S.M. Ibrahima,"Physicochemical, mechanical, microstructure and durability characteristics of alkali activated Egyptian slag", Constr. Build.Mater., 69 (30); (2014), pp. 60-72.
[3] G.A. Blengini, T. Di Carlo, "The changing role of life cycle phases, subsystems and materials in the LCA of low energy buildings", Energy and Buildings, 42 (6); (2010), pp. 869–880.
[4] C. Becchio, S.P. Corgnati, A. Kindinis, S. Pagliolico, "Improving environmental sustainability of concrete products: investigation on MWC thermal and mechanical properties", Energy and Buildings, 41 (11); (2009), pp. 1127–1134.
[5] B. A. Sabrah, S. Abd El-Aleem, H. Gouda, "Physico-Mechanical and Chemical Properties of Composite Cement Containing High Percentages of Mechanically Activated Egyptian Slag", International Journal of Engineering Research & Technology (IJERT), 3 (9), (2014), pp. 1446-1457.
[6] Cahit Bilim, OkanKarahan, Cengiz Duran Atis , Serhan Ilkentapar, "Influence of admixtures on the properties of alkali-activated slag mortars subjected to different curing conditions", J. Mat. Desig.,." 44, (2013), pp. 540–47.
[7] Hung Chi-Che and Chang Jiang-Jhy, "The influence of mixture variables for the alkali-activated slag concrete on the properties of concrete", J. Marine. Sci. Tech., 21(3); (2013), pp. 229-237.
[8] H. El Didamony, H.H. Assal, , T.M. El Sokkary, H.A. Abdel Gawwad, "Kinetics and physico-chemical properties of alkali activated blast-furnace slag/basalt pastes", J.Hous. Buld.Res. Cent., 8; (2012), pp. 170–176.
[9] M.A. Cincotto, A.A. Melo, W.L. Repette, "Effect of different activators type and dosages and relation to autogenous shrinkage of activated blast furnace slag cement", in: G. Grieve, G. Owens (Eds.), Proceedings of the 11th International Congress on the Chemistry of Cement, Durban, .4; (2003), pp. 1878–1888.
[10] D. Krizan, B. Zivanovic, "Effects of dosage and modulus of water glass on early hydration of alkali–slag cements", J.Cem. Concr. Res., 32; (2002), pp. 1181–1188.
[11] Y. Li, Y. Sun, "Preliminary study on combined-alkali–slag paste materials", J.Cem. Concr. Res., 30; (2000), pp. 963–966.
[12] A. A. Melo Neto, M.A. Cincotto, W. Repette, "Drying and autogenous shrinkage of pastes and mortars with activated slag cement." J.Cem.Concr. Res., 38; (2008), pp. 565–574.
[13] T. Kutti, L.Berntsson, S.Chandra, "Shrinkage of cements with high content of blast-furnace slag", In: Proc 4th CANMET/ACI IntConf on Fly Ash, Slag, and Natural Pozzolans in Concrete, Istanbul, Turkey; 1992, pp. 615–625.
[14] E. Douglas, A. Bilodeau, V.M. Malhotra, "Properties and durability of alkaliactivated slag concrete", J. ACI Mater., 89; (1992), pp. 509–516.
[15] T. Bakharev, J.G. Sanjayan, Y.B. Cheng, "Effect of admixtures on properties of alkali activated slag concrete." J.Cem. Concr. Res., 30; (2000), pp. 1367–1374.
[16] Z. Lou, Q. Ye , H. Chen, Y. Wang, J. Shen , "Hydration of MgO in clinker and its expansion property." J. Chin. Ceram. Soc., 26; (1998), pp. 430–436.
[17] P. Gao, S. Wu, P. Lin, Z. Wu, M. Tang, "Morphology of MgO hydration products under different curing conditions", J.Chin. Inorg. Chem., 23; (2007), pp. 1063–1068.
[18] E.E. Holt, "Early age autogenous shrinkage of concrete", Tech. Res. Cent. Finland; (2001), pp. 446.
[19] M. Ben Haha, B. Lothenbach, G. Le Saout, F. Winnefeld, "Influence of slag chemistry on the hydration of alkali-activated blast-furnace slag—Part I: Effect of MgO", J. Cem. Concr. Res., 41; (2011), pp. 955–963.
[20] W. Shen, Y. Wang, T. Zhang, M. Zhou, J. Li, X. Cui, "Magnesia modification of alkaliactivated slag fly ash cement", J. Wuhan.Univ.Technol-Mater. Sci., 26; (2011), pp. 121–125.
[21] M.A. Shand, "The Chemistry and Technology of Magnesia", John Wiley & Sons, Ltd., Hoboken, New Jersey; (2006).
[22] Fei Jin, Kai Gu, Abir Al-Tabbaa "Strength and drying shrinkage of reactive MgO modified alkali-activated slag paste." J. Constr. Build. Mater., 51; (2014), pp. 395–404.
[23] Frost Veronika Vágvölgyi, L. Frost Ray, Matthew Hales, Ashley Locke, JánosKristóf, Erzsébet Horváth, "Controlled rate thermal analysis of hydromagnesite", J. Therm. Anal. Calorim., 92(3);(2008), pp. 893-897.
[24] H. El Didamony, H.H Assal, T.M. El Sokkary, H.A. Abdel Gawwad, "Physico-chemical properties of alkali activated slag pastes", J.Hous. Buld.Res. Cent., 6; (2010), pp. 47-55.
[25] H. El-Didamony, A.A. Amer, , T.M. El-Sokkary, H. Abd-El-Aziz, "Effect of substitution of granulated slag by air-cooled slag on the properties of alkali activated slag", J. Ceram. Intern., 39; (2013), pp. 171–181.
[26] ASTM C109M, "Standard test method for compressive strength of hydraulic cement mortars", (2012).
[27] ASTM C490, "Standard practice for use of apparatus for the determination of length change of hardened cement paste, mortar, and concrete", (2007).
[28] L. Mo, M. Deng, M. Tang, "Effects of calcination condition on expansion property of MgO-type expansive agent used in cement-based materials."J.Cem.Concr. Res., 40 (3); (2010), pp. 437–446.
[29] M. Liska, "Properties and applications of reactive magnesia cements in porous blocks", PhD thesis.University of Cambridge.
[30] F. Jin, A. Al-Tabbaa, "Thermogravimetric study on the hydration of reactive MgO and silica mxiture at room temperature", J. Thermochim. Acta., 566; (2013), pp. 162–168.
[31] S. A. Bernal, J.L. Provis, V. Rose, R.M. Gutiérrez, "High-resolution X-ray diffraction and fluorescence microscopy characterization of alkali-activated slag–metakaolin binders", J. Am. Ceram. Soc., 96; (2013), pp. 1951–1957.
[32] T. Zhang, C.R. Cheeseman, L.J. Vandeperre, "Development of low pH cement systems forming magnesium silicate hydrate (MSH)", J.Cem. Concr. Res., 41; (2011), pp. 439–442.

[33] M.D.R Brew, F.P. Glasser, "Synthesis and characterisation of magnesium silicate hydrate gels", J.Cem. Concr. Res., 35; (2005), pp. 85–98.
[34] G. Tartaglione, D.Tabuani, G. Camino, "Thermal and morphologicalcharacterisation of organically modified sepiolite", J.MicroporousMesoporous Mater., 107; (2008), pp. 161–168.
[35] P. Parashar, , V. Sharma, D.D Agarwal, N. Richhariya, "Rapid synthesis of hydrotalcite with high antacid activity." J. Mater.Lett.,74;(2012), pp. 93–95.
[36] F. Demir, B. Donmez, H. Okur, F. Sevim, "Calcination kinetic of magnesite from thermogravimetric data." J. Chem. Eng. Res. Des., 81; (2003), pp. 618–622.
[37] P. Duxson, J.L. Provis , J.S.J van Deventer, "Geopolymers: Structures, processing, properties and industrial applications, Geopolymer synthesis kinetics", Wood head Publishing, Abingdon UK; (2009), pp. 118-136.

Table 1: Chemical compositions of hydromagnesite and granulated blast-furnace slag (GBFS), wt., %

Oxide, %	*SiO_2*	*Al_2O_3*	*Fe_2O_3*	*CaO*	*MgO*	*Na_2O*	*K_2O*	*SO_3*	*TiO_2*	*P_2O_5*	*L.O.I*	*Total*
Hydromagnesite	0.09	0.08	0.01	0.4	42.95	-	0.18	0.04	-	0.03	56.19	99.94
GBFS	37.81	13.14	0.23	38.70	7.11	1.03	0.19	1.19	0.40	0.17	-	99.97

Table 2: Mix composition of blended slag- cement pastes

Mix symbol	MgO wt. %	GBFS, wt. %	SH, wt.%	LSS wt.%	Water/ Solid ratio	Calcination temperature, °C
M0	0	100	3	3	0.30	-
M5-550	5	95	3	3	0.30	550
M10-550	10	90	3	3	0.30	550
M15-550	15	85	3	3	0.30	550
M5-1000	5	95	3	3	0.30	1000
M5-1250	5	95	3	3	0.30	1250

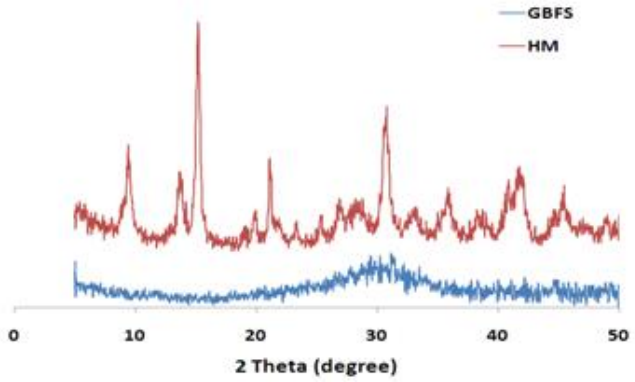

Figure 1: XRD pattern of hydromagnesite and slag samples

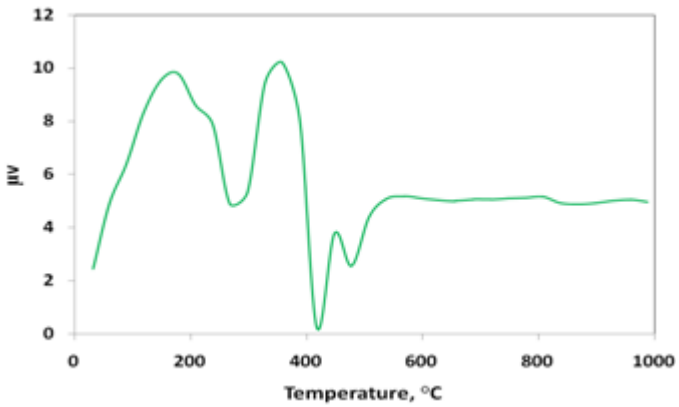

Figure 3: DTA thermogram of hydromagnesite

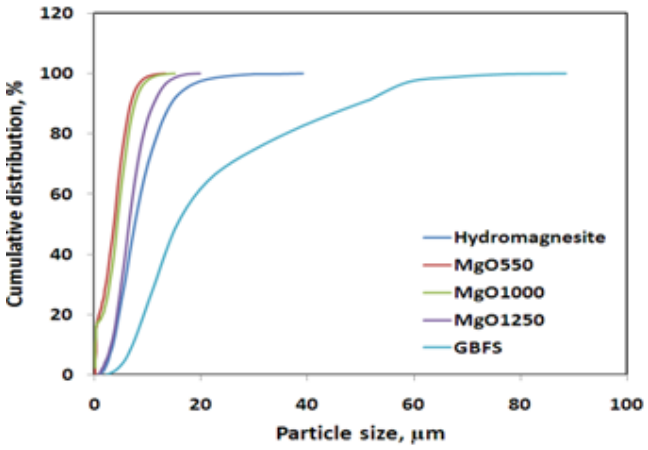

Figure 2: Particle sizes distribution of hydromagnesite and MgO_{550}, MgO_{1000} and MgO_{1250}

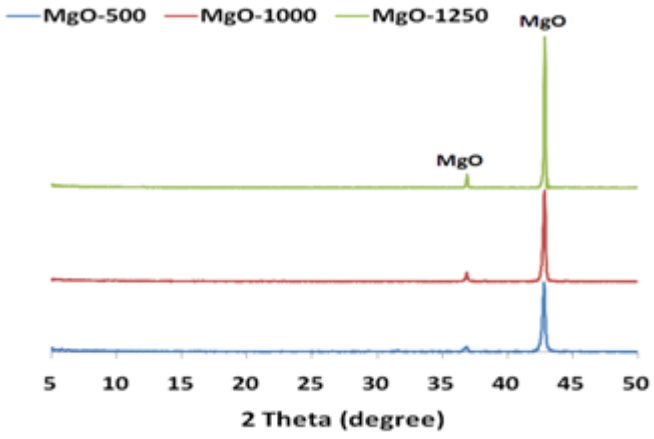

Figure 4: XRD pattern of MgO calcined at 550, 1000 and 1250°C

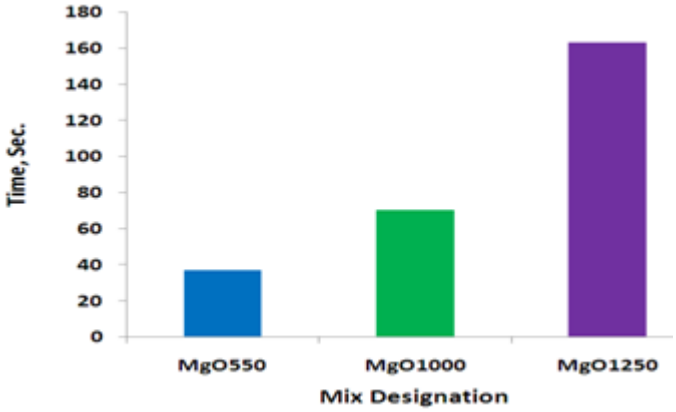

Figure 5: Determination reactivity of MgOs by acetic acid test

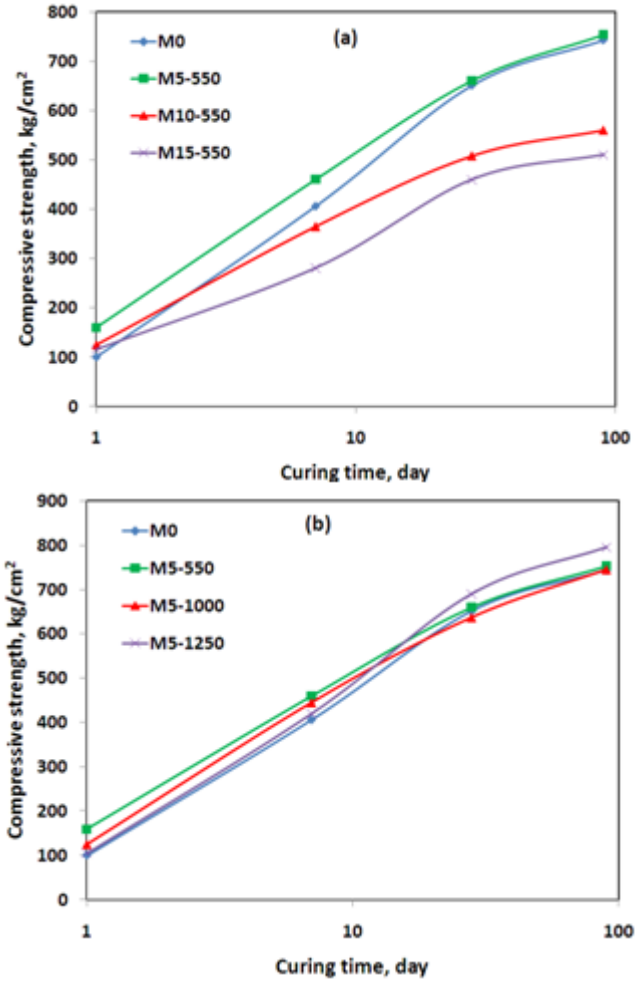

Figure 6: Compressive strength of AAS bleded with (a) 5, 10 and 15% of MgO_{550} and (b) 5% of MgO_{550}, MgO_{1000} and MgO_{1250}

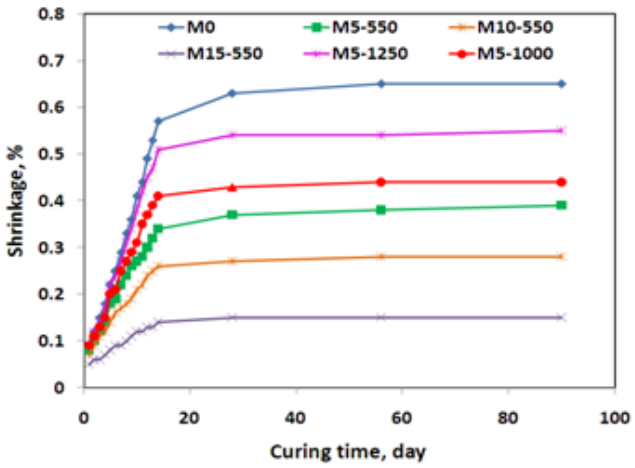

Figure 7: Dring shrinkage of AAS containing 0, 5, 10 and 15 wt., % MgO_{550} as well as 5wt., % MgO

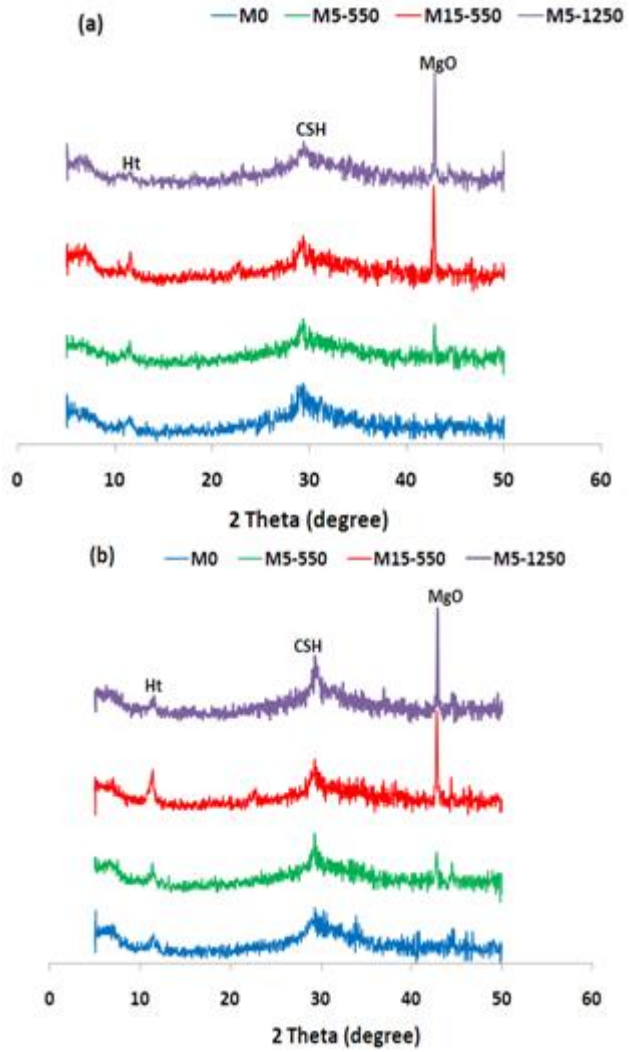

Figure 8: XRD diffractograms of reference specimens and AAS-MgO blends after (a) 1 day and (b) 28 days

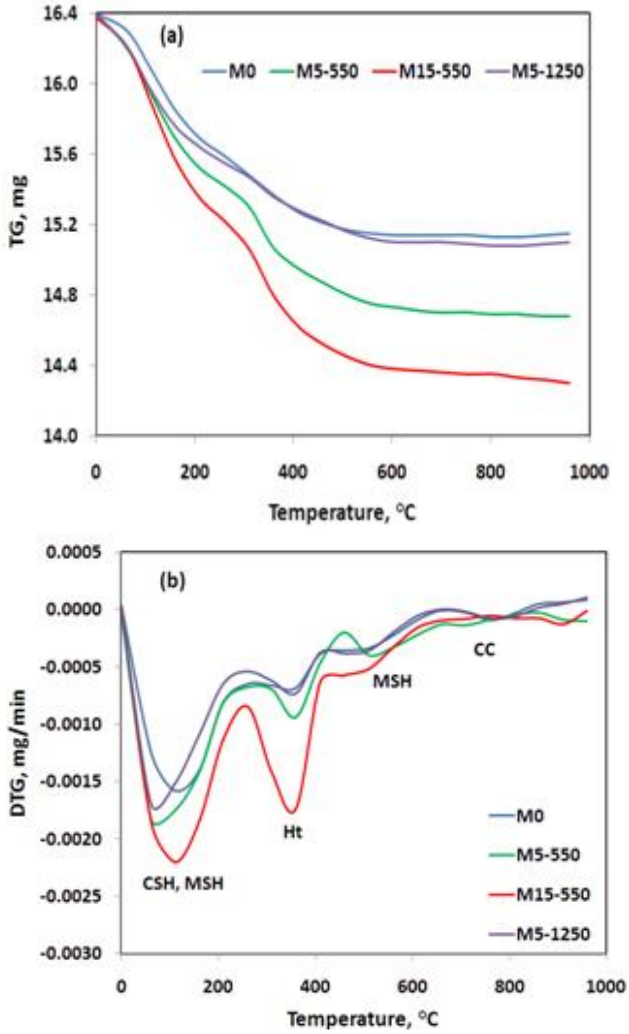

Figure 9: TGA (a) and DTG (b) of AAS and AAS-MgO blends after 1 day

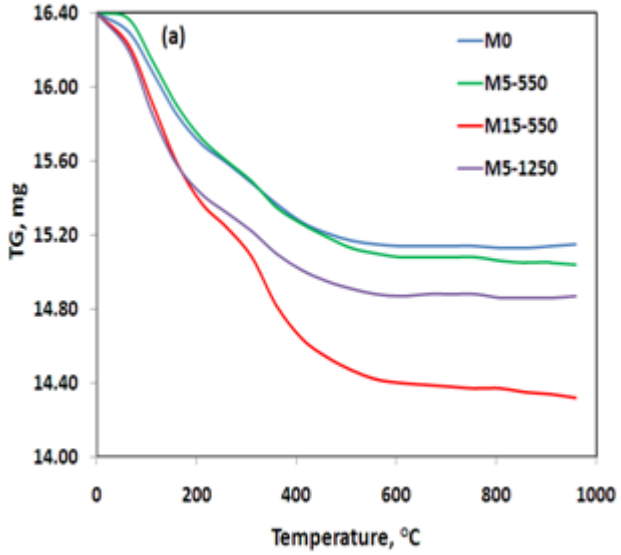

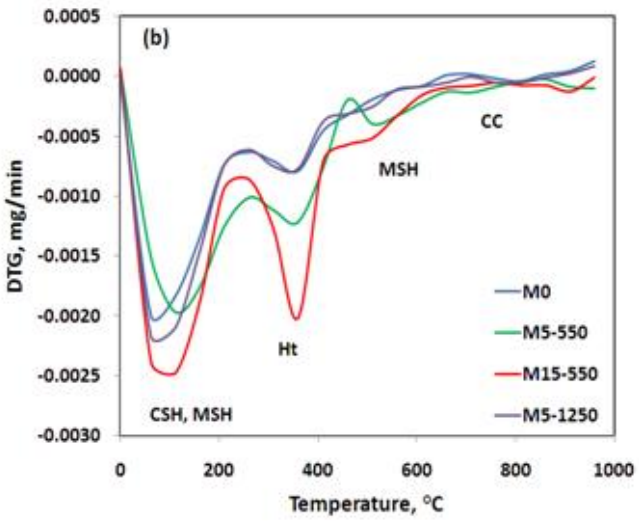

Figure 10: TGA (a) and DTG (b) of AAS and AAS-MgO blends after 28 days

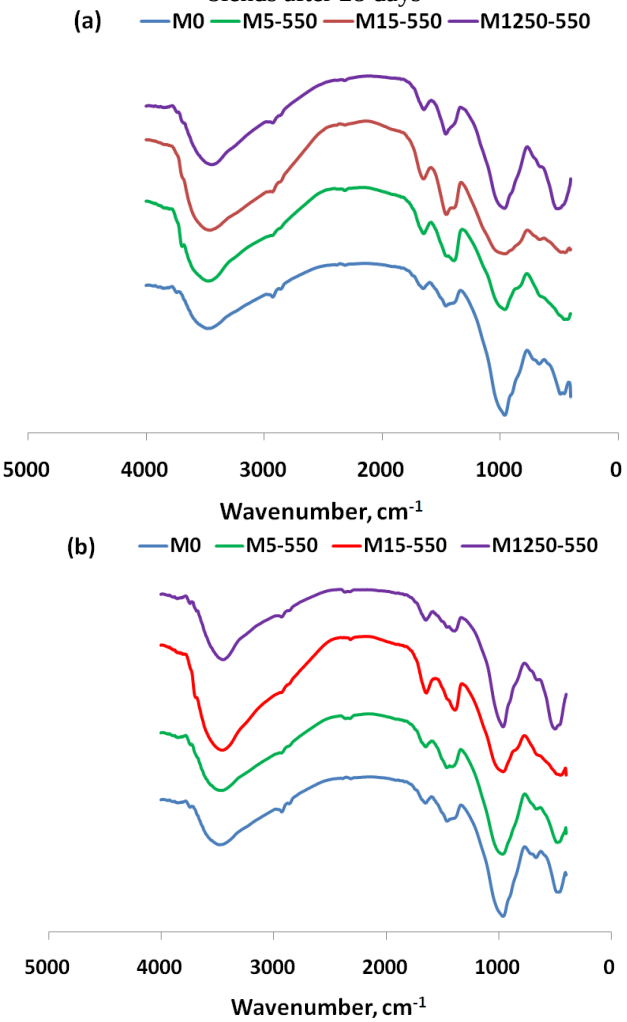

Figure 11: FTIR spectra of AAS and ASS-MgO blends after (a) 1 day and (b) 28 days